Laser-Induced Breakdown Spectroscopy for space exploration applications : Influence of the ambient pressure on the calibration curves prepared from soil and clay samples.

Béatrice Sallé[a], David A. Cremers[b], Sylvestre Maurice[c,*], Roger C. Wiens[d]

[a] *CNRS, INSU, 3 rue Michel Ange, BP 287, 75766 Paris Cedex 16, France.*

[b] *Los Alamos National Laboratory, Advanced Chemical Diagnostics and Instrumentation Group, MS J565, Los Alamos, NM 87545, USA.*

[c] *Observatoire Midi-Pyrénées, Centre d'Etude Spatiale des Rayonnements, 9 avenue du Colonel Roche, 31400 Toulouse, France.*

[d] *Los Alamos National Laboratory, Space and Atmospheric Sciences Group, MS D466, Los Alamos, NM 87545, USA.*

* Corresponding author. *E-mail address:* sylvestre.maurice@cesr.fr

Abstract

Recently, there has been an increasing interest in the LIBS (Laser-Induced Breakdown Spectroscopy) technique for stand-off detection of geological samples for use on landers and rovers to Mars, and for other space applications. For space missions, LIBS analysis capabilities must be investigated and instrumental development is required to take into account constraints such as size, weight, power and environmental atmosphere (pressure and ambient gas) imposed on flight instruments. In this paper, we study the in-situ LIBS method at reduced pressure (7 Torr CO_2 to simulate the Martian atmosphere) and near vacuum (50 mTorr to simulate the Moon or asteroids' pressure) as well as at atmospheric pressure in air

(for Earth conditions and comparison). We show the influence of the ambient pressure on the calibration curves prepared from certified soil and clay pellets. In order to detect simultaneously all the elements commonly observed in terrestrial soils, we used an Echelle spectrometer. The results are discussed in terms of calibration curves, measurement precision, plasma light collection system efficiency and matrix effects.

Keywords: Laser-Induced Breakdown Spectroscopy; Reduced pressure; Matrix effects; Soils; Clays; Space applications.

1. Introduction

The LIBS (Laser-Induced Breakdown Spectroscopy) technique has been proposed as a new method that could be installed on landers and rovers for stand-off detection of geological samples on the planetary surfaces [1-4]. LIBS is based on the focusing of a high-power pulsed laser beam (≥ 1 GW/cm^2) onto a sample surface leading to the creation of a plasma composed of excited species which emit light. Plasma collection, followed by spectral dispersion and detection, permits identification of the elements present in the sample using their characteristic spectral lines and quantitative analysis. This technique has been applied to many samples such as solid samples even in hostile environments [5], liquids [6,7], gases [8] and, environmental and geological samples [9-12]. For space exploration, this method possesses several advantages compared to other techniques which have been used on past and current missions (examples at Mars: X-Ray Fluorescence on the Viking 1 and 2 missions [13,14], Alpha-Proton-X-Spectroscopy on the Pathfinder mission [15] and the Mars Exploration Rover missions in progress): stand-off analysis capability [16,17], no sample preparation, rapid analysis (few minutes), simultaneous multi-elemental detection (major, minor and trace elements), ability to measure the composition of weathered layers and the underlying bulk rock composition through depth profiling. For space applications, LIBS analysis capabilities must be investigated and instrumental development is required to take into account constraints such as size, weight, power and environmental atmosphere (pressure and ambient gas) imposed on flight instruments. Because of different environmental atmospheres expected on Mars, the Moon, asteroids, studies are needed to understand analytical requirements and performance under such conditions. In this paper, we characterize the in-situ LIBS method at reduced pressure (7 Torr CO_2 for Mars) and near vacuum (50 mTorr for the Moon and asteroids) as well as at atmospheric pressure in air (585 Torr for Los Alamos atmospheric

conditions and comparison). This characterization is important because the excitation properties of the LIBS plasma are strongly dependent on the pressure of the surrounding atmosphere, which can have a strong effect on the detection of elements in a solid [3,18]. We studied the influence of the ambient pressure on the calibration curves of elements commonly observed in terrestrial soils including Al, Ba, Ca, Cr, Fe, K, Li, Mg, Mn, Na, Ni, Si, Sr, Ti, and prepared from certified soil and clay pellets. Results are presented for in-situ analysis describing measurement precision for quantitative analysis and matrix effects. We also studied the possibility of using the non time-resolved spectra acquisition at low pressures and the influence of the plasma light collection system on the analytical results obtained at reduced pressures.

2. Experimental setup

For testing in-situ analysis by LIBS at different pressures, we used the experimental setup presented in Fig. 1. Special care was taken to reproduce the experimental conditions expected in space exploration, especially for the laser in terms of wavelength, repetition rate and energy. A Q-switched Nd:YAG laser (Spectra Physics) operating at 1064 nm and 10 Hz was focused with a 150 mm focal length lens (L_1, 25 mm diameter) onto the sample surface. The laser energy used for plasma formation was 40 mJ which is considered to be in the energy range achievable by a compact laser likely to be incorporated on landers or rovers. The samples were placed in a chamber where the pressure could be adjusted between atmospheric pressure and 30 mTorr. The chamber could also be filled with a flowing stream of CO_2 gas in order to simulate the Martian atmosphere. Light from the plasma was collected out of laser axis and focused with a 100 mm focal length lens (L_2, 50 mm diameter) onto a fused silica optical fibre (length = 1 m, core diameter = 1 mm). The end of this fibre was directly

connected to the entrance slit of an Echelle spectrograph (ESA 3000, LLA, Gmbh) equipped with an Intensified Charge-Coupled Device (ICCD) camera detector system (KAF 1000, Kodak). The advantage of this device is its ability to simultaneously collect the entire 200 to 780 nm spectral range with a resolution of ~10000. Since chromatic aberration existed in this setup, the optical fibre was positioned to give the optimal signal across the largest part of the spectral range.

For space applications, compact integrated spectrograph and detection systems are available commercially but because of their small size and mass, these devices have no intensified detectors, and the associated temporal gating of the emission signal can not be used [19]. An evaluation of these commercial compact systems is in progress in the laboratory [20]. For these reasons, we used the ESA 3000 Echelle spectrograph without temporal resolution and with a wide time gating (1 ms) in order to record the plasma emission on all its lifetime. Results obtained in such conditions were compared with those recorded with a time delay between ICCD camera aperture and the laser pulse. The time resolution was controlled by a programmable pulse delay generator (DG 535, Stanford Research Systems). The intensifier gain was maintained to a constant value in all experiments (gain G = 1800, maximum gain of the system = 4000). The gain was systematically fixed at 1800 because the commercial compact system suitable for space investigation has no intensifier and a gain of 1800 almost corresponds to a non intensified system. The plasma light was integrated on 50 laser shots, a reasonable number for a compact laser likely to be incorporated on a rover. Each spectrum was replicated 6 times on a fresh surface of the sample.

Calibration curves were prepared for elements including Al, Ba, Ca, Fe, Mg, Mn, Na, Pb, Si, Sr and Ti using a series of certified samples provided by Brammer Standard Company, Inc, USA: soils (GBW 07301, GBW 07304 to GBW 07312, GBW 07404) and clays (GBW 03101a, GBW 03102, GBW 03102a, GBW 03103, GBW 03115, IPT 28). Each point

displayed on calibration graphs is a mean value obtained from 6 spectra. The error bars were obtained with a confidence of 95%, inducing a Student *t* factor equal to 2.447. They were calculated from the formula $\frac{t \times \sigma}{\sqrt{n}}$ with *n* the number of replicates and σ the standard deviation.

3. Results and discussion

3.1. Effect of time resolution and pressure on spectra

A number of LIBS studies have used time resolution of the emission signal to enhance signal to background ratios by recognizing that different decay rates characterize the continuum and atomic emission processes [21]. Spectral interference may also be minimized by taking into account the differing relaxation times between different elements [22]. For LIBS analysis applied to space exploration, we are considering a very compact grating type spectrograph integrated in a single package with a CCD detector [19]. This detector is not gated as are the more sophisticated gated-intensifier CCD arrays often used for LIBS. Signal acquisition without temporal resolution is planned to be employed for a LIBS flight instrument. Thus, we wanted to know if analytically useful spectra could be obtained without gating the detection system. We compared in Fig. 2 spectra obtained from one soil (reference GBW 07301) without temporal resolution and with a time delay of 1 µs between the ICCD camera aperture and the laser pulse, at atmospheric pressure and at 7 Torr of CO_2 (gate width = 1 ms). In this figure, the spectra were normalized to the maximum intensity of the spectrum acquired without time resolution at atmospheric pressure. The time delay of 1 µs was chosen because it gave the highest signal to background ratio for the majority of studied elements at atmospheric pressure and 7 Torr of CO_2. At atmospheric pressure, a continuum is emitted at

the beginning of the plasma (Fig. 2a). The LIBS spectra of Al and Ca lines show pressure broadening. With time resolution (Fig. 2b), the continuum emission and the line widths decrease. At 7 Torr of CO_2 (Fig. 2c), the continuum emission is reduced compared to atmospheric pressure and the width of lines is lower. With time resolution (Fig. 2d), the emission signal becomes very low and not all the lines are detected. The width of detectable lines (like Fe, Ti, Sr, Mn) shows little change with time resolution and pressure. These results are consistent with those obtained in Ref. [23] at high pressure: the elements that are present at concentrations of more than a few percent by weight in the sample (e.g. Al and Ca) and that have transitions originating from lower energy upper levels (< 3.15 eV) that end at or near the ground state energy level (< 0.02 eV) are those that show strong effects of a pressure increase by broadening/self-absorption. The observed Mn, Sr and Ti lines also have upper energy levels < 3.13 eV that all end in the ground state but these show no significant broadening/self-absorption with pressure increase and these elements are present in the sample at concentrations lower than a percent. Elements that are present at concentrations higher than a few percent which do not exhibit the strong effects of pressure increase (e.g. Fe and Si) all have upper energy levels which are relatively high (> 4.55 eV) and the transitions end in upper energy levels (> 1.48 eV). The concentration of elements and the energy levels of the transition appear to be the main factors affecting broadening and self-absorption.

Table 1 presents the signal to background ratio obtained for the Si line (390.57 nm) at atmospheric pressure and 7 Torr of CO_2 without temporal resolution and with a time delay of 1 μs. Without temporal resolution, the signal to background ratio is greater at 7 Torr than at atmospheric pressure. The use of time delay allows to increase the signal to background ratio and this is more significant at atmospheric pressure. These results show that analytically useful spectra can be obtained without gating the detection system, preferably at reduced pressures.

3.2. Effect of time resolution on calibration curves

Fig. 3 depicts calibration curves of Sr (407.7 nm) prepared from soils without temporal resolution and with a time delay of 1 µs at atmospheric pressure and at 7 Torr of CO_2. In the two pressure conditions, the slope of the calibration curves (which represents the sensitivity) without time resolution is higher than the slope with time delay. This indicates that lower detection limits can be obtained without temporal resolution. This result can be explained by the constant gain chosen for all experiments. Of course, the use of a higher gain of the ICCD with a 1 µs time delay would lead to more sensitive results. But to reproduce as close as possible the commercial apparatus suitable for space applications, the intensifier gain must remain at a constant value. The difference of slope between the calibration curves obtained with and without temporal resolution is greater at 7 Torr (factor of 4 difference) than at atmospheric pressure (factor of 1.3). The fast expansion of the plasma at reduced pressure could induce a rapid escape of excited species from the observation region and a greater loss of emission signal with time delay than at atmospheric pressure. Fig. 4a demonstrates that, in air at atmospheric pressure, the Relative Standard Deviation (RSD) which corresponds to a mean value for all the studied concentrations, is approximately the same with and without temporal resolution. At 7 Torr of CO_2, the RSD is generally lower without temporal resolution (Fig. 4b).

With the pressure decrease, using no temporal resolution seems to be a good solution for quantitative analysis because we obtain more emission signal and thus more sensitivity, and because the RSD is better. From this study, we can conclude that non-gated-intensifier detectors can be used for LIBS analysis at reduced pressures for space applications. In the

following studies with ESA 3000 Echelle spectrograph, we used no time delay and a gate width of 1 ms as acquisition parameters of plasma light.

3.3. Influence of the pressure on calibration curves

Fig. 5 shows the calibration curves, obtained at three different pressures for Mg (major element, line at 280.2 nm) and Sr (minor element, line at 407.7 nm). Comparison of the curves shows a systematic decrease in the slope of the curve (the analytical sensitivity) with decreased pressure. It can be observed that it is impossible to obtain a linear calibration curve for Mg at atmospheric pressure. The same behaviour is also obtained for the elements Al, Ba, Ca, Cr, Fe, Mn, Si. It is not only due to self-absorption at high concentrations but we can suppose that it is also due to the matrix effects. With the pressure decrease, the linear regression coefficient of the calibration curves becomes better. At 7 Torr of CO_2 and high concentrations, the curve shows a relative loss in intensity due to self-absorption of the strong 280.2 nm Mg line. A linear calibration curve can be obtained at high concentrations through the use of a weaker Mg emission line. Fig. 6 demonstrates that RSD is the lowest at 7 Torr of CO_2.

The emission intensity changes produced by the ambient pressure can be explained by three main factors, namely, changes in the vaporized amount by plasma shielding, changes in plasma temperature by the absorption of laser radiation, and changes in the plasma expansion [24, 25]. To give an idea of the plasma excitation temperatures, they were measured by the usual method of the Boltzmann plot slope [26]. We used the set of Fe lines available in the 358-377 nm spectral region. The lines, the corresponding energy levels, the statistical weights and the transition probabilities are listed in Table 2 [27]. Fig. 7 shows the Boltzmann plots obtained for a soil containing 10.71% of Fe_2O_3 at the three different pressures. We deduced an

excitation temperature of 10695 K at atmospheric pressure, 9440 K at 7 Torr of CO_2 and 13400 K at 50 mTorr. Taking into account the uncertainties on the statistical weights and transition probabilities (between 10 and 25% depending on the line [27]), we can conclude that there is no major difference between the plasma temperature obtained at atmospheric pressure and at 7 Torr. An increase of the plasma temperature is observed at 50 mTorr. Because of higher excitation temperature and lower plasma density at reduced pressure, the laser energy absorption by the plasma due to the Inverse Bremsstrahlung (IB) is lower than at atmospheric pressure. At reduced pressure, a large part of incident laser energy interacts directly with the sample surface. At atmospheric pressure, the larger part of the laser energy is used to heat the plasma. The laser energy reaching the sample surface and the amount of vaporized sample decrease. Furthermore in our experiments, higher excitation temperature and vaporized amount do not directly result in higher emission intensities. This is due to the fact that the plasma expansion should be taken into account. At atmospheric pressure, the ambient air confines the spark near the target surface, causing it to occupy a small volume. The hot plasma results not only in analytical emission but also in an intense background continuum. At reduced pressure, the lack of pressure allows the increase of the spark size and the rapid expansion of plasma can cause a weakening of the signal intensity due to the rapid escape of emissive species from the observation region.

The plasma formed at reduced pressure gives more intense emissions (if we do not take into account the light collection system) and we can think that a more intense emission results in greater stability and repeatability, explaining the better RSD obtained at 7 Torr of CO_2. This could also explain the better linear regression obtained for calibration curves with the pressure decrease. We can also argue that with the pressure decrease, there are fewer collisions between atoms in the plasma resulting in a decrease of the matrix effects and in better calibration curves. At 50 mTorr, the observed increase of the RSD can be attributed to

the low detected emission signal which makes difficult the calculation of background subtracted signal.

These results show that Martian pressure is favourable for quantitative analysis by the LIBS technique because we observe a better linear regression of calibration curves and better RSD at 7 Torr of CO_2. The systematic decrease in the slope of the curves with decreased pressure indicates the need for enhanced instrument capabilities at pressures in the 50 mTorr range.

3.4. Influence of plasma light collection system on calibration curves

The difference in the plasma expansion (or in the plasma volume) with the ambient pressure has implications for the method of light collection, e.g. optical fibre directly positioned near the plasma or imaging of the plasma light on fibre optic end. We compared the previous results (obtained by imaging the plasma light on the optical fibre end) with results obtained by placing the fibre optic near the plasma. Fig. 8 shows the calibration curves of Mg (280.2 nm) prepared from soils for this last light collection condition and the three different pressures. The calibration curves show the same aspect as the calibration curves obtained by imaging the plasma light on the optical fibre (Fig. 5a). A loss of signal is observed for all the pressures when the optical fibre is placed near the plasma. This loss is more important at atmospheric pressure. Fig. 9 indicates that for all pressures studied, the RSD is higher when the optical fibre is placed near the plasma. The RSD increase is more important at atmospheric pressure. These observations could be explained by the fact that with the optical fibre placed near the plasma (about 15 cm), the light is collected in a smaller solid angle than with the optical configuration of 1:1 magnification. With the pressure

decrease, the plasma volume increases and only a portion of the plasma could be collected by the optical fibre with the two light collection setups.

As a conclusion, the loss of signal with decreasing pressure has implications for the use of LIBS at low pressures (e.g., in the 50 mTorr range): it indicates that analysis at stand-off distances in such conditions will require more efficient light collection and recording methods. With the two systems of plasma light collection and for all the studied elements, we obtained calibration curves with better linear regression and the best RSD for a pressure of 7 Torr in CO_2 (Fig. 5,6,8,9). It could be explained as a result of lower absorption of laser energy in the plasma and fewer collisions between the atoms at reduced pressures inducing a more stable plasma and a decrease of matrix effects.

3.5. Matrix effects

Fig. 10 shows a comparison of calibration curves obtained for Ca (393.3 nm) in soils and clays at different pressures. At atmospheric pressure and 7 Torr of CO_2 (Fig. 10 a and b), the emission signals obtained in the soil and clay matrices are different. The emission intensity for the soil matrix is greater than the intensity for the clay matrix. At atmospheric pressure, Wisbrun et al. [28] found that emissions from sand were greater than those from soil, which is consistent with Eppler et al. observation [29] of greater slopes for calibration curves obtained from the sand matrices than the slopes for the soil matrices. These last authors showed that neither aerosol production above the sand and soil samples nor absorptivity nor particle size affected the observed differences in emissions from the sand and soil matrices. They found that the electron density of the plasma obtained from pure sand was lower than those obtained from pure soil and that the plasma temperature, however, remained constant. They suggested that elements found at appreciable concentrations in the soil matrix

may have produced the increased electron density of the plasma formed on soil, since these elements all have lower ionization potentials than Si and O, the major components of the sand matrix. The greater electron density of the plasma formed on soil reduced the concentration of ions in the plasma through ion-electron recombination, decreasing the observed emission intensity from the ion lines. But this analysis could not explain the differences in the slopes of the calibration curves for the neutral species. In our measurements, the elements found at appreciable concentrations in soils and clays are similar, only the relative concentrations are different. The previous explanation can not be applied to our study, and other mechanisms are operating that affect emission intensities. Further experiments are needed to understand the difference of emission intensity between soils and clays at atmospheric pressure.

Fig. 10 shows that the difference in emission intensities of plasmas formed on soil and clay samples decreases with the pressure decrease and becomes non significant at 50 mTorr (Fig. 10c). The same behaviour is observed for all studied elements. This means that the matrix effects are pressure dependent. Chemical matrix effects can be due to interactions (collisions, electric fields) of atoms closer together. As the pressure is reduced, the number of collisions between atoms in the plasma decreases so the matrix effects are reduced. Another explanation for the decrease of matrix effects at lower pressures could be different interaction regimes at different pressures. Inverse Bremsstrahlung (IB) is more effective with the use of infrared laser wavelength and with denser plasmas. As already mentioned, this effect is more important at atmospheric pressure than at reduced pressure. Thus near vacuum, we can suppose a direct interaction between the laser and the sample. With the high laser power density, the physical and chemical properties of the samples do not influence the laser-matter interaction process. With the pressure increase, the plasma density increases inducing a more effective IB process. A greater part of laser energy is absorbed in the plasma inducing a shielding of the sample surface from the laser radiation and a decrease of the vaporized matter

amount in the plasma. The larger part of the laser energy is used to heat the plasma which itself can produce additional heating of the sample surface by radiation and by convection. The interaction is dominated by a laser-plasma and plasma-surface interaction regime. The heating of the sample by the plasma must be material dependent, explaining the different emission intensities obtained for soils and clays at atmospheric pressure and at 7 Torr of CO_2. From these results, we can conclude that reduced pressures are favourable for LIBS analysis of elements found in different matrices, as the matrix effects are less important at lower pressures.

4. Conclusion

This paper was focused on the use of the LIBS technique for analysis of geological samples on planetary surfaces. We have studied the influence of the ambient pressure (50 mTorr for the Moon or asteroids, 7 Torr of CO_2 for Mars, and atmospheric pressure for the Earth) on the calibration curves prepared from certified soil and clay pellets. The results show that calibration curves can be obtained without temporal resolution of the emission signal at reduced pressure. The best linear regression coefficient and the best repeatability are obtained at 7 Torr of CO_2 for Martian conditions. We have also shown that the method of plasma light collection had implications on the analytical results obtained at reduced pressures. We have observed a systematic decrease in the slope (the sensitivity) of the curves with decreasing pressure when the plasma light was imaged on an optical fibre end. This tendency was not observed when the plasma light was collected with an optical fibre placed near the spark. This indicates the need for enhanced instrument capabilities in the area of plasma light collection at lower pressures. Finally, comparison of the curves obtained in soils and clays showed that matrix effects were less important when the ambient pressure was lower. Quantitative LIBS

analysis of elemental abundances regardless of the chemical matrices will be favoured in the atmospheric pressure environments of the Moon and asteroids.

Acknowledgments

B. Sallé thanks the Los Alamos National Laboratory (LANL) for the support given during this work and the CNES, the French national institute for space research, which has permitted this exchange program.

References

[1] A.K. Knight, N.L. Scherbarth, D.A. Cremers, M.J. Ferris, Characterization of Laser-Induced Breakdown Spectroscopy (LIBS) for applications to space exploration, Appl. Spectrosc. 54 (2000) 331-340.

[2] R.C. Wiens, R.E. Arvidson, D.A. Cremers, M.J. Ferris, J.D. Blacic, F.P. Seelos IV, K.S. Deal, Combined remote mineralogical and elemental identification from rovers: Field and laboratory tests using reflectance and laser-induced breakdown spectroscopy, J. Geophys. Res.107 (2002) 10.1029/2000JE001439.

[3] R. Brennetot, J.L. Lacour, E. Vors, A. Rivoallan, D. Vailhen, S. Maurice, Mars Analysis by Laser-Induced Breakdown Spectroscopy (MALIS): Influence of Mars atmosphere on plasma emission. Study of factors influencing plasma emission with the use of Doehlert designs, Appl. Spectrosc. 57 (2003) 744-752.

[4] F. Colao, R. Fantoni, V. Lazic, A. Paolini, G.G. Ori, L. Marinangeli, A. Baliva, Investigation of LIBS feasibility for in-situ planetary exploration: An analysis on Martian rock analogues, Planetary and Space Science 52 (2004) 117-123.

[5] P. Fichet, P. Mauchien, C. Moulin, Determination of impurities in uranium and plutonium dioxides by laser induced breakdown spectrocopy, Appl. Spectrosc. 53 (1999) 1111-1117.

[6] P. Fichet, P. Mauchien, J.F. Wagner, C. Moulin, Quantitative elemental determination in water and oil by laser induced breakdown spectroscopy, Anal. Chim. Acta 429 (2001) 269-278.

[7] M. Tran, Q. Sun, B. Smith, J.D. Winefordner, Direct determination of trace elements in terephthalic acid by laser induced breakdown spectroscopy, Anal. Chim. Acta 419 (2000) 153-158.

[8] M. Hanafi, M.M. Omar, Y.E.E.-D. Gamal, Study of laser-induced breakdown spectroscopy of gases, Radiat. Phys. Chem. 57 (2000) 11-20.

[9] J. Bublitz, C. Dölle, W. Schade, A. Hartmann, R. Horn, Laser induced breakdown spectroscopy for soil diagnostics, Eur. J. Soil Sci. 52 (2001) 305-312.

[10] M.C. Boiron, J. Dubessy, N. André, A. Briand, J.L. Lacour, P. Mauchien, J.M. Mermet, Analysis of mono-atomic ions in individual fluid inclusions by laser-produced plasma emission spectroscopy, Geochim. Cosmochim. Acta 55 (1991) 917-923.

[11] D. Ohnenstetter, W.L. Brown, Compositional variation and primary water contents of differentiated interstitial and included glasses in boninites, Contrib. Mineral. Petrol. 123 (1996) 117-137.

[12] C. Fabre, M.C. Boiron, J. Dubessy, A. Moissette, Determination of ions in individual fluids by laser ablation optical emission spectroscopy, J. Anal. At. Spectrom. 14 (1999) 913-922.

[13] B.C. Clark, A.K. Baird, H.J. Rose Jr., P. Toulmin, R.P. Christian, W.C. Kelliher, A.J. Castro, C.D. Rowe, K. Keil, G.R. Huss, The Viking X ray fluorescence experiment: analytical methods and early results, J. Geophys. Res. 82 (1977) 4577-4594.

[14] J. Bruckner, G. Dreibus, R. Rieder, H. Wanke, Lunar Planet. Sci. XXXII, The Lunar and Planetary Institute, Houston TX (2001) abstr. 1293.

[15] R. Rieder, T. Economou, H.Wanke, A. Turkevich, J. Crisp, J. Bruckner, D. Dreibus, H.Y. McSween Jr., The chemical composition of martian soil and rocks returned by the mobile alpha proton x-ray spectrometer: preliminary results from the x-ray mode, Science 278 (1997) 1771-1774.

[16] D.A. Cremers, The analysis of metals at a distance using laser-induced breakdown spectroscopy, Appl. Spectrosc. 41 (1987) 572-578.

[17] S. Palanco, J.M. Baena, J.J. Laserna, Open-path laser-induced plasma spectrometry for remote analytical measurements on solid surfaces, Spectrochim. Acta Part B 57 (2002) 591-599.

[18] M. Kuzuya, O. Mikami, Effect of argon pressure on spectral emission of a plasma produced by a laser microprobe, JAAS 7 (1992) 493-497.

[19] S.I. Gornushkin, I.B. Gornushkin, J.M. Anzano, B.W. Smith, J.D. Winefordner, Effective normalization technique for correction of matrix effects in Laser-Induced Breakdown Spectroscopy detection of magnesium in powdered samples, Appl. Spectrosc. 56 (2002) 433-436.

[20] B. Sallé, D.A. Cremers, K. Benelli, J. Busse, R.C. Wiens, S. Maurice, R. Walters, Evaluation of a compact spectrograph/detection system for a LIBS instrument for in-situ and stand-off detection, Lunar Planet. Sci. XXXV, The Lunar and Planetary Institute, Houston TX (2004) abstr. 1263.

[21] N. André, C. Geertsen, J.L. Lacour, P. Mauchien, S. Sjostrom, UV laser ablation optical emission spectrometry on aluminum alloys in air at atmospheric pressure, Spectrochim. Acta Part B 49 (1994) 1363-1372.

[22] M. Milan, J.M. Vadillo, J.L. Laserna, Removal of air interference in Laser_Induced Breakdown Spectrometry monitored by spatially and temporally resolved charge-coupled device measurements, JAAS 12 (1997) 441-444.

[23] Z.A. Arp, D.A. Cremers, R.D. Harris, D.M. Oschwald, G.R. Parker Jr., D.M. Wayne, Feasibility of generating a useful laser-induced breakdown spectroscopy plasma on rocks at high pressure: preliminary study for a Venus mission, Spectrochim. Acta Part B 59 (2004) 987-999.

[24] Y. Iida, Effects of atmosphere on laser vaporization and excitation processes of solid samples, Spectrochim. Acta Part B 45 (1990) 1353-1367.

[25] J.M. Vadillo, J.M. Fernandez Romero, C. Rodriguez, J.J. Laserna, Effect of plasma shielding on laser ablation rate of pure metals at reduced pressure, Surf. Interface Anal. 27 (1999) 1009-1015.

[26] W. Lochte-Holtgreven, Evaluation of plasma parameter, in W. Lochte-Holtgreven (Ed.), Plasma Diagnostics. North-Holland, Amsterdam, 1968, Chapter 3, p. 135.

[27] Handbook of chemistry and physics, 62nd edition, CRC Press, 1981-1982, p. E349-E351.

[28] R. Wisbrun, I. Schechter, R. Niessner, H. Schröder, K. Kompa, Detector for trace elemental analysis of solid environmental samples by laser plasma spectroscopy, Anal. Chem. 66 (1994) 2964-2975.

[29] A.S. Eppler, D.A. Cremers, D.D. Hickmott, M.J. Ferris, A.C. Koskelo, Matrix effects in the detection of Pb and Ba in soils using Laser-Induced Breakdown Spectroscopy, Appl. Spectrosc. 50 (1996) 1175-1181.

LIST OF TABLES

Table 1: Signal to background ratio for the Si line (390.57 nm) obtained at different pressures, without temporal resolution and with a time delay of 1 μs.

Table 2: Spectroscopic data of iron lines.

Table 1

Signal to background ratio for the Si line (390.57 nm) obtained at different pressures, without temporal resolution and with a time delay of 1 µs.

Pressure	585 Torr	7 Torr of CO_2
Delay 0	6	10
Delay 1 µs	178	82

Table 2
Spectroscopic data of iron lines.

Line (nm)	Excitation energy (cm^{-1})	Statistical weight g	Transition probability A
358.119	34844	13	1.02
358.6984	35856	5	0.17
360.5454	49727	9	0.65
360.668	49434	13	0.84
360.8859	35856	5	0.814
361.016	50342	13	0.5
361.8768	35612	7	0.73
362.1462	49604	11	0.52
363.15	35257	9	0.52
364.7842	34782	11	0.292
368.22	55754	5	1.7
368.7456	34040	9	0.0801
370.55	27395	7	0.032
370.9246	34329	7	0.156
371.99	26875	11	0.163
372.25	27560	5	0.049
372.7619	34547	5	0.225
373.48	33695	11	0.902
373.71	27167	9	0.142
374.34	34692	5	0.156
374.56	27395	7	0.115
374.83	27560	3	0.1525
375.82	34329	7	0.634
376.7	34692	3	0.64

FIGURE CAPTIONS

Fig. 1. Experimental setup used for LIBS at different pressures. L_1=focusing lens; L_2=collection lens; OF=Optical Fibre; VC=Vacuum Chamber; VP=Vacuum Pump.

Fig. 2. LIBS spectra obtained from one soil at 400 nm a) in air without temporal resolution; b) in air with a time delay of 1 µs; c) at 7 Torr of CO_2 without temporal resolution; d) at 7 Torr of CO_2 with a time delay of 1 µs.

Fig. 3. Calibration curves of Sr prepared from soils without and with temporal resolution a) at atmospheric pressure; b) at 7 Torr of CO_2.

Fig. 4. Relative Standard Deviation obtained from calibration curves in soils without and with temporal resolution a) at atmospheric pressure; b) at 7 Torr of CO_2.

Fig. 5. Calibration curves prepared from soils at different pressures a) for Mg and b) for Sr.

Fig. 6. Relative Standard Deviation obtained from calibration curves in soils at three different pressures.

Fig. 7. Boltzmann plots obtained for a soil containing 10.71% of Fe_2O_3 at different pressures (I: emission intensity, λ: wavelength, g: statistical weight, A: transition probability).

Fig. 8. Calibration curves prepared from soils at different pressures for Mg (280.2 nm) when the optical fibre is placed near the plasma.

Fig. 9. Relative Standard Deviation (RSD) obtained from calibration curves in soils at three different pressures (no crosshatching corresponds to imaging of plasma light on the optical fibre end and crosshatching corresponds to direct plasma light collection with an optical fibre placed near the plasma).

Fig. 10. Calibration curves prepared from certified soils and clays a) at atmospheric pressure; b) at 7 Torr of CO_2 and c) at 50 mTorr.

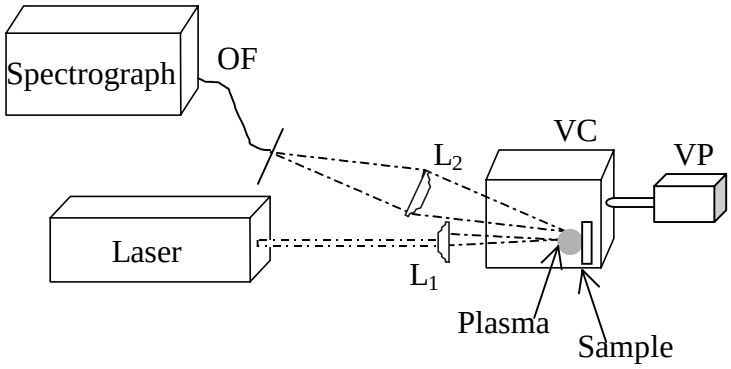

Fig. 1. Experimental setup used for LIBS at different pressures. L_1=focusing lens; L_2=collection lens; OF=Optical Fibre; VC=Vacuum Chamber; VP=Vacuum Pump.

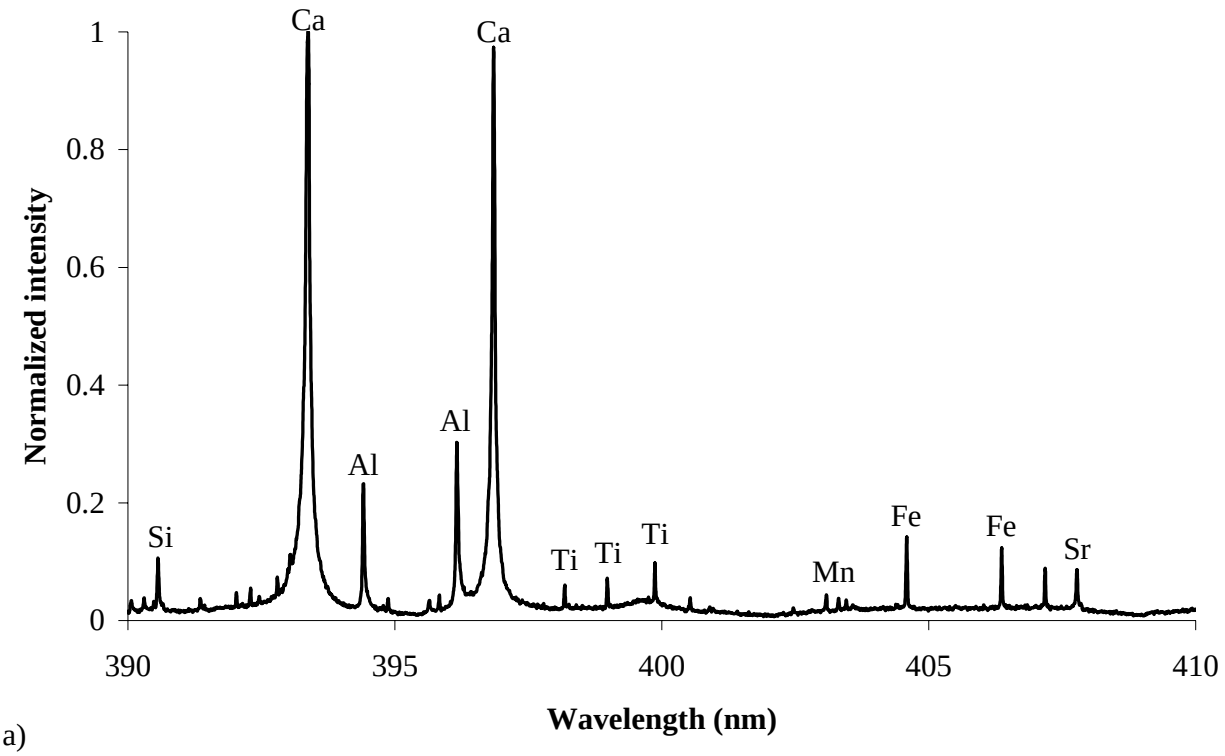
Ca
Ca
Al
Al
Si
Ti
Ti
Ti
Mn
Fe
Fe
Sr
Normalized intensity
Wavelength (nm)
0
0.2
0.4
0.6
0.8
1
390
395
400
405
410

a)

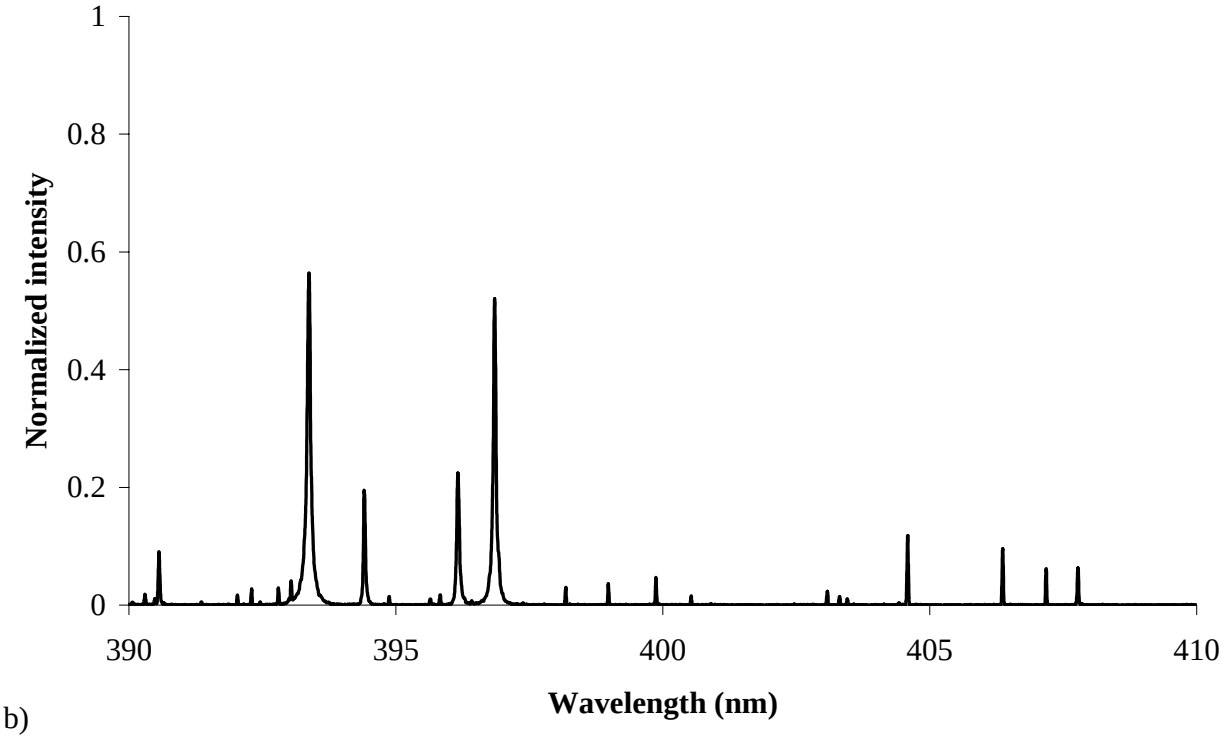
Normalized intensity
Wavelength (nm)
0
0.2
0.4
0.6
0.8
1
390
395
400
405
410

b)

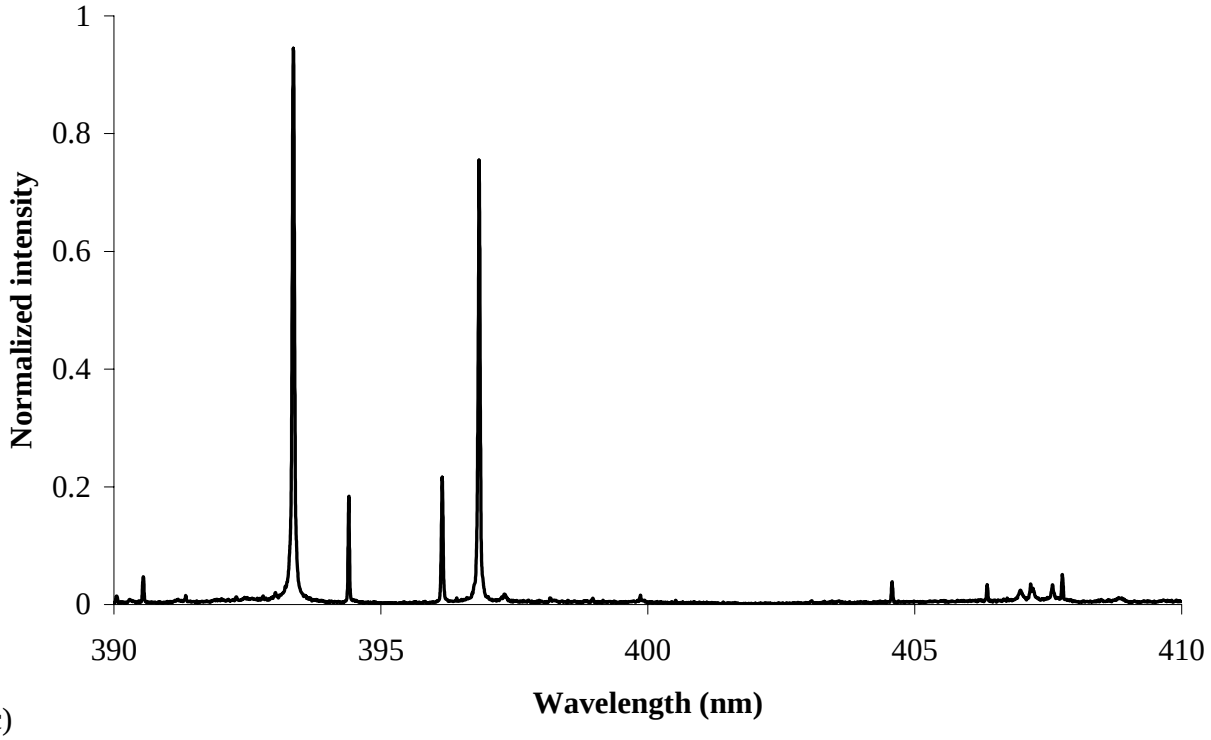
1
0.8
0.6
0.4
0.2
0
Normalized intensity
390
395
400
405
410
Wavelength (nm)

c)

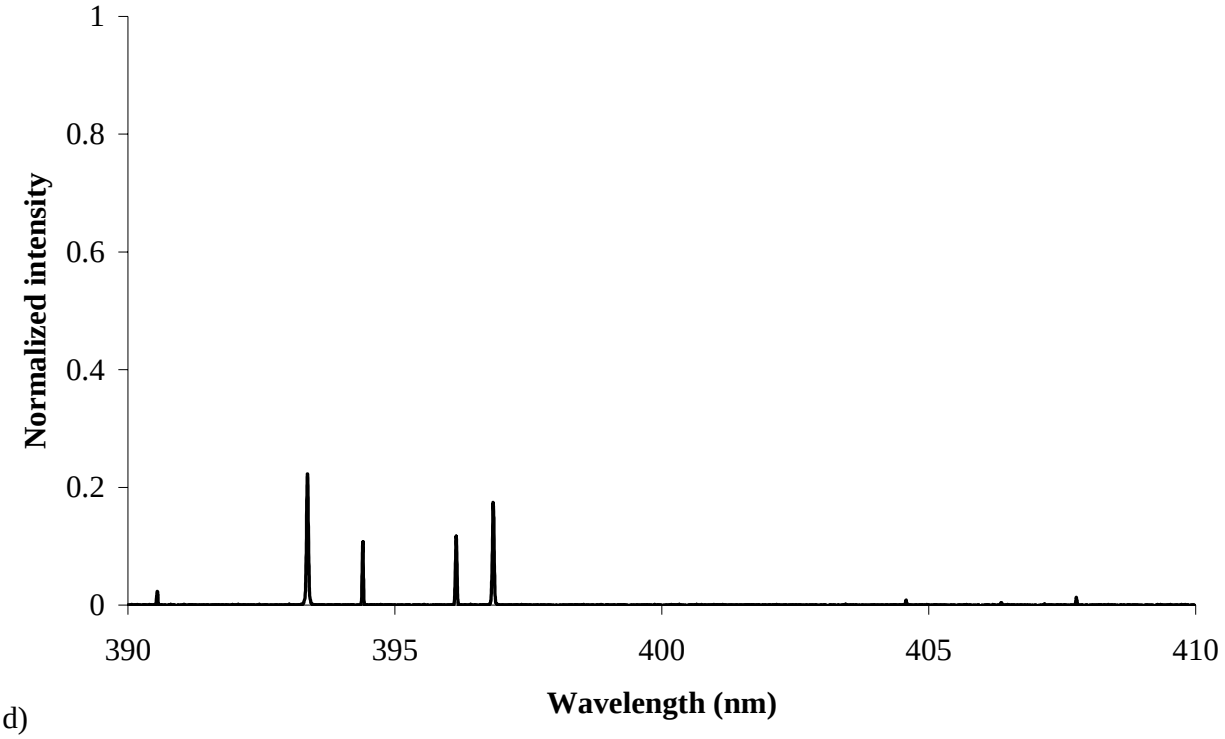
1
0.8
0.6
0.4
0.2
0
Normalized intensity
390
395
400
405
410
Wavelength (nm)

d)

Fig. 2. LIBS spectra obtained from one soil at 400 nm a) in air without temporal resolution; b) in air with a time delay of 1 µs; c) at 7 Torr of CO_2 without temporal resolution; d) at 7 Torr of CO_2 with a time delay of 1 µs.

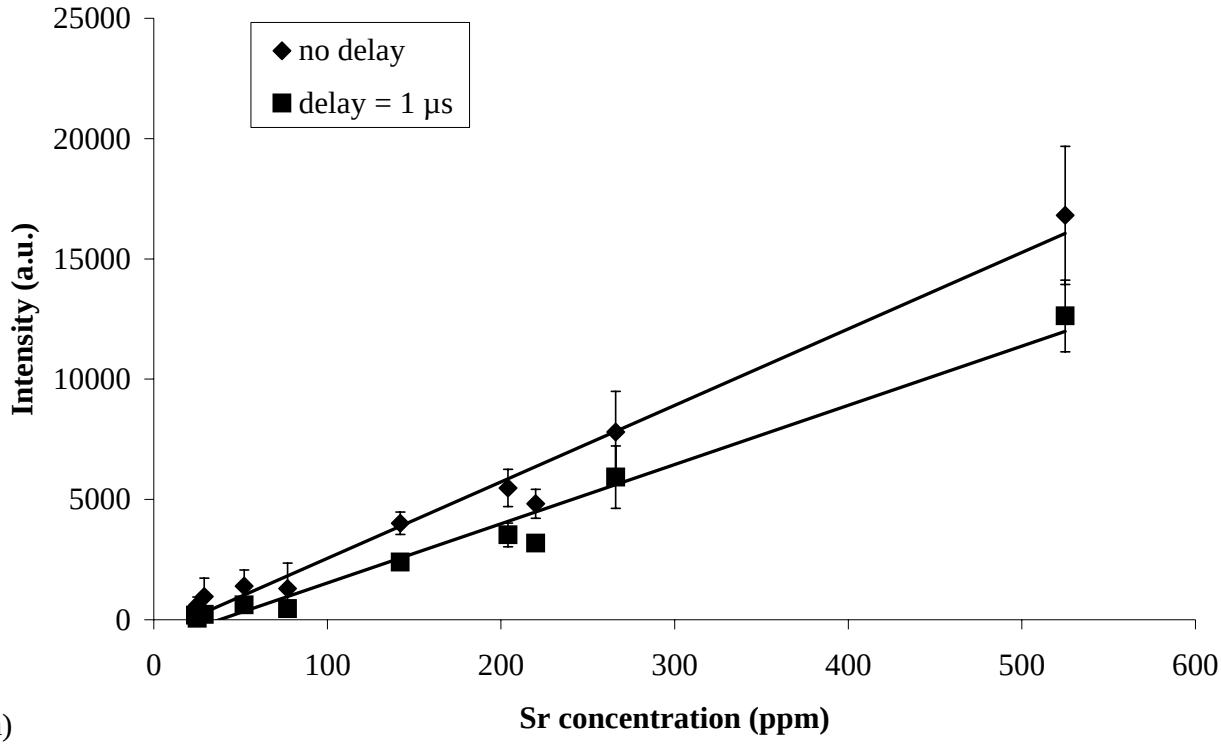

a)

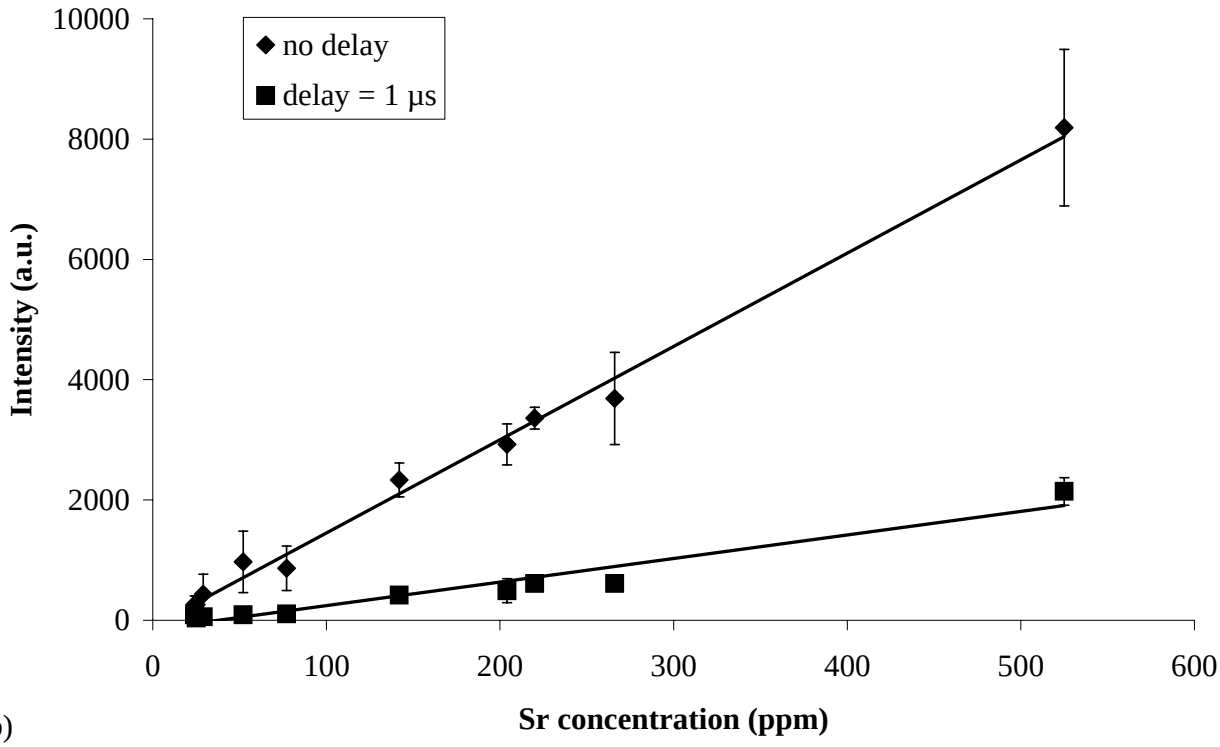

b)

Fig. 3. Calibration curves of Sr prepared from soils without and with temporal resolution a) at atmospheric pressure; b) at 7 Torr of CO_2.

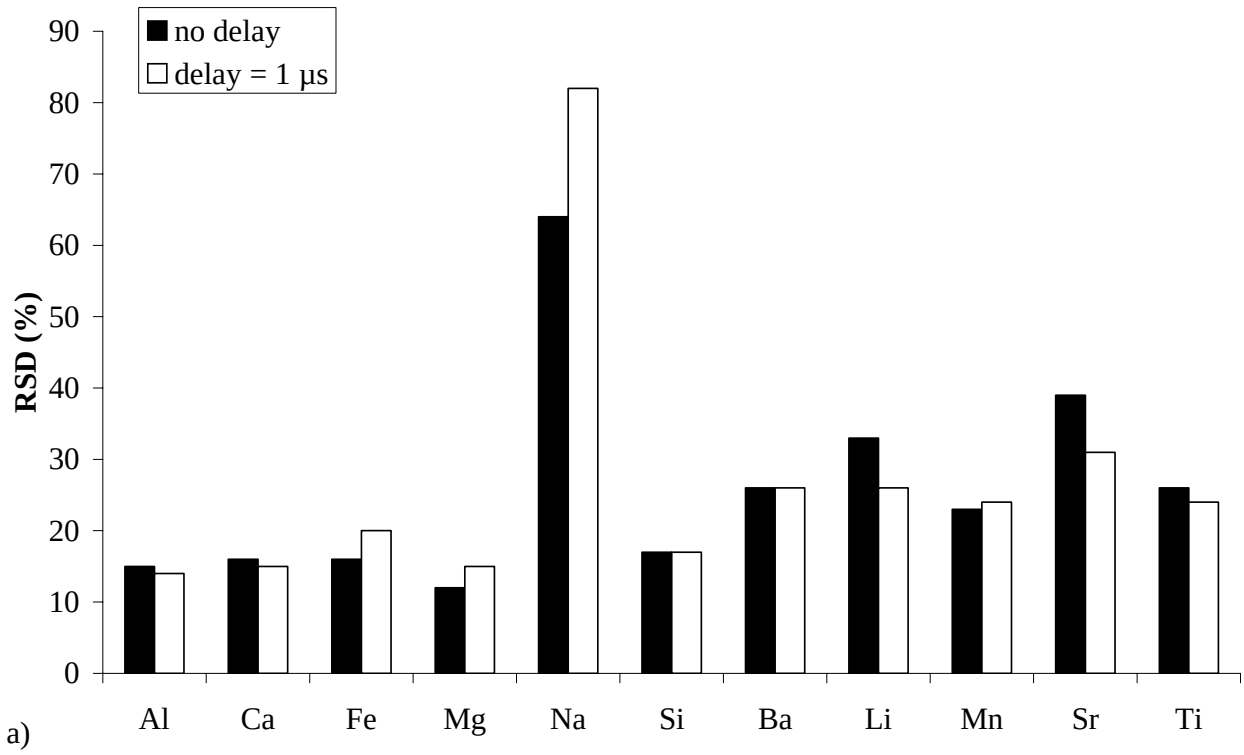

a)

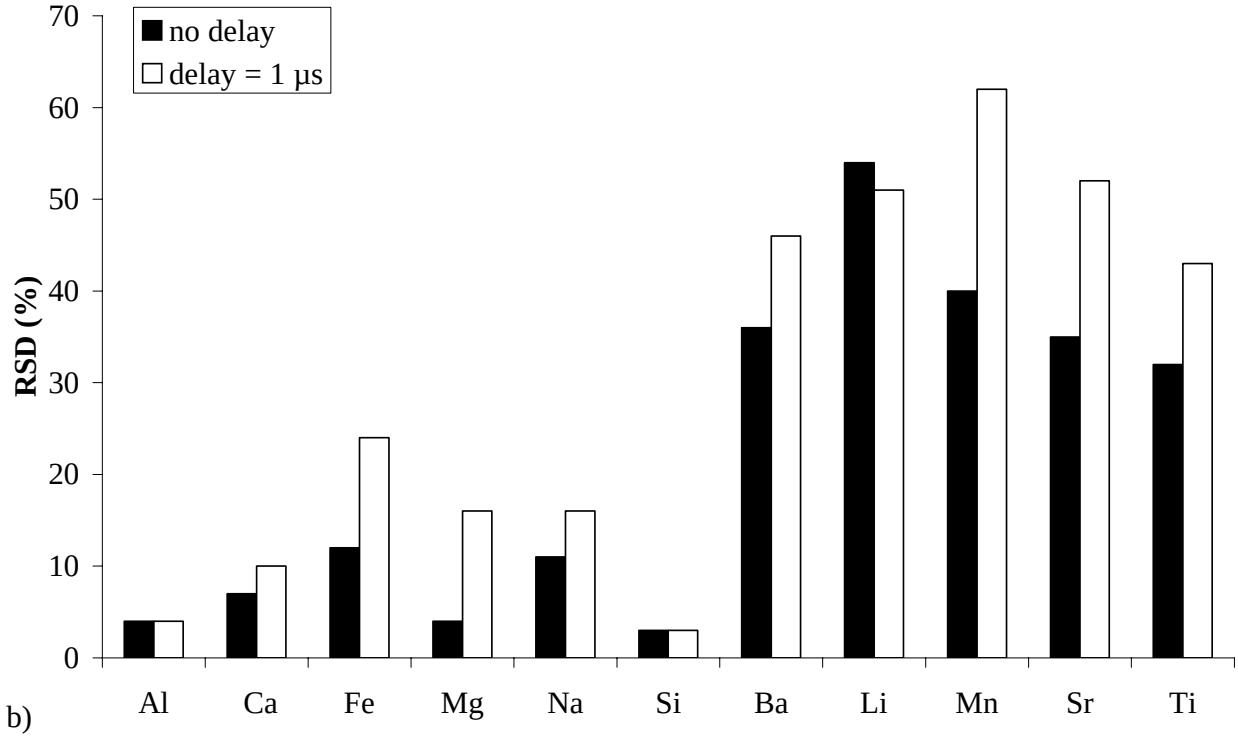

b)

Fig. 4. Relative Standard Deviation obtained from calibration curves in soils without and with temporal resolution a) at atmospheric pressure; b) at 7 Torr of CO_2.

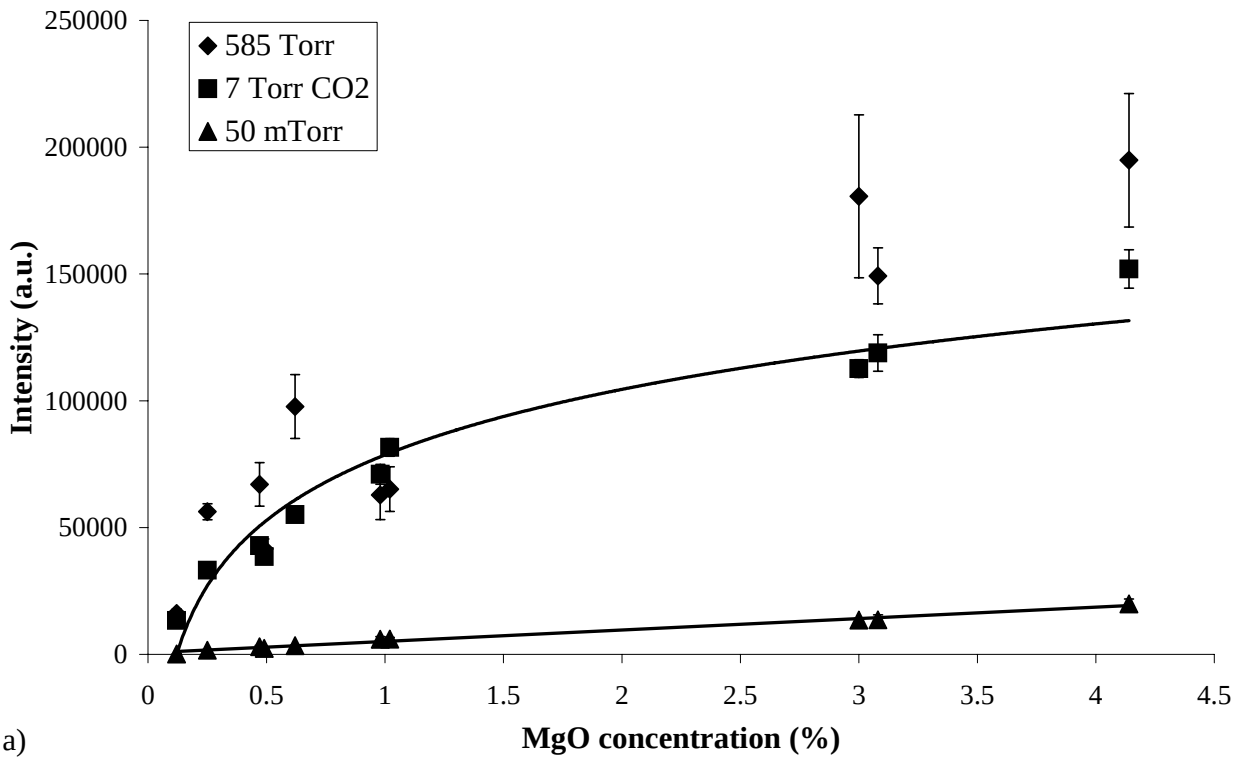

a)

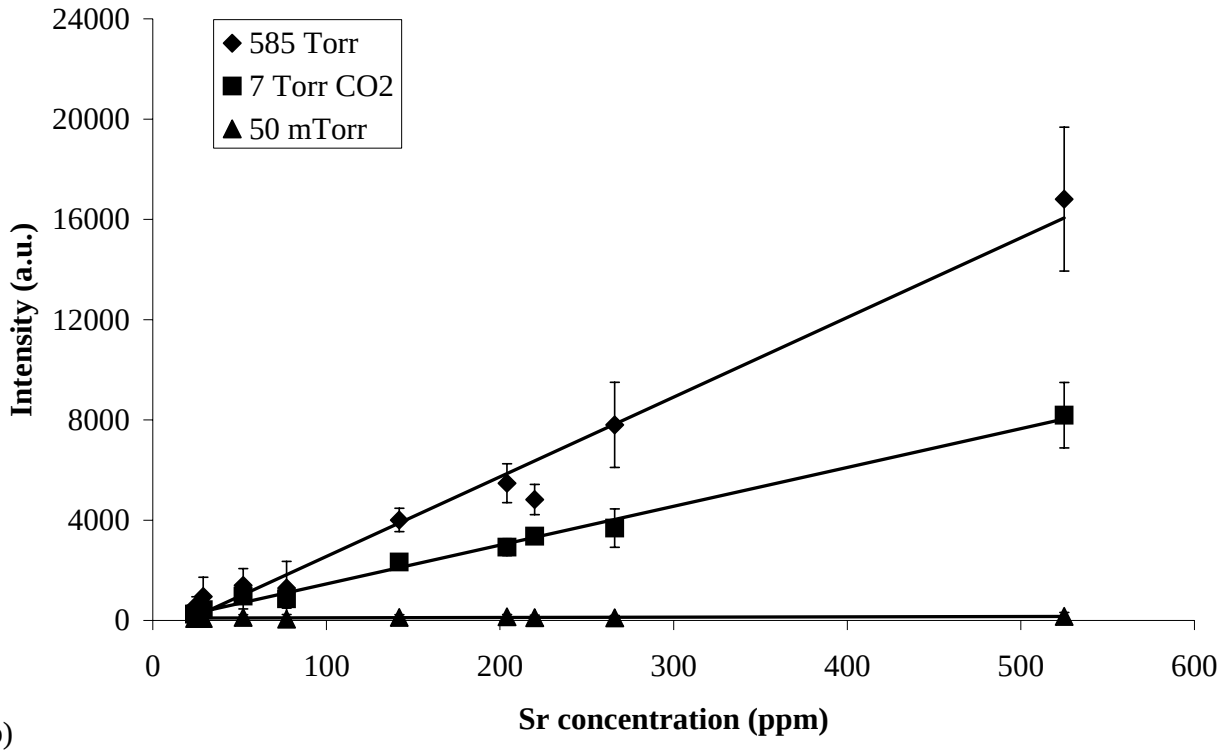

b)

Fig. 5. Calibration curves prepared from soils at different pressures a) for Mg and b) for Sr.

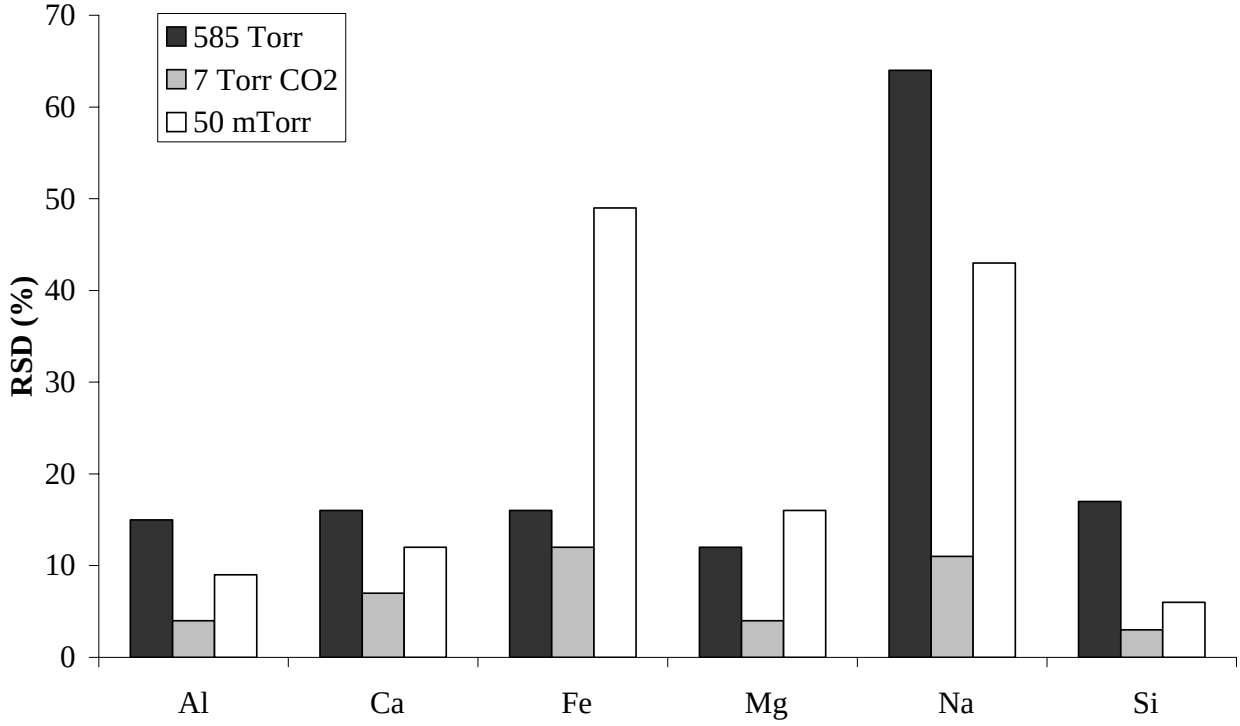

Fig. 6. Relative Standard Deviation obtained from calibration curves in soils at three different pressures.

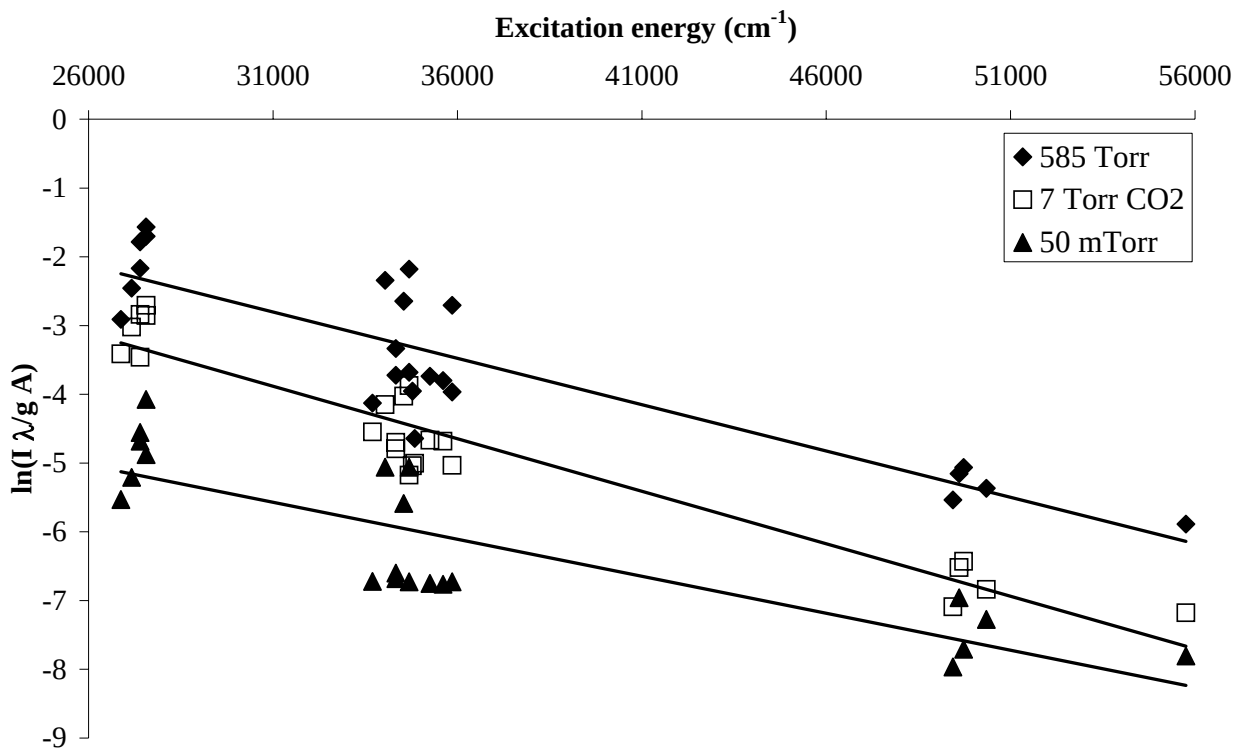

Fig. 7. Boltzmann plots obtained for a soil containing 10.71% of Fe_2O_3 at different pressures (I: emission intensity, λ: wavelength, g: statistical weight, A: transition probability).

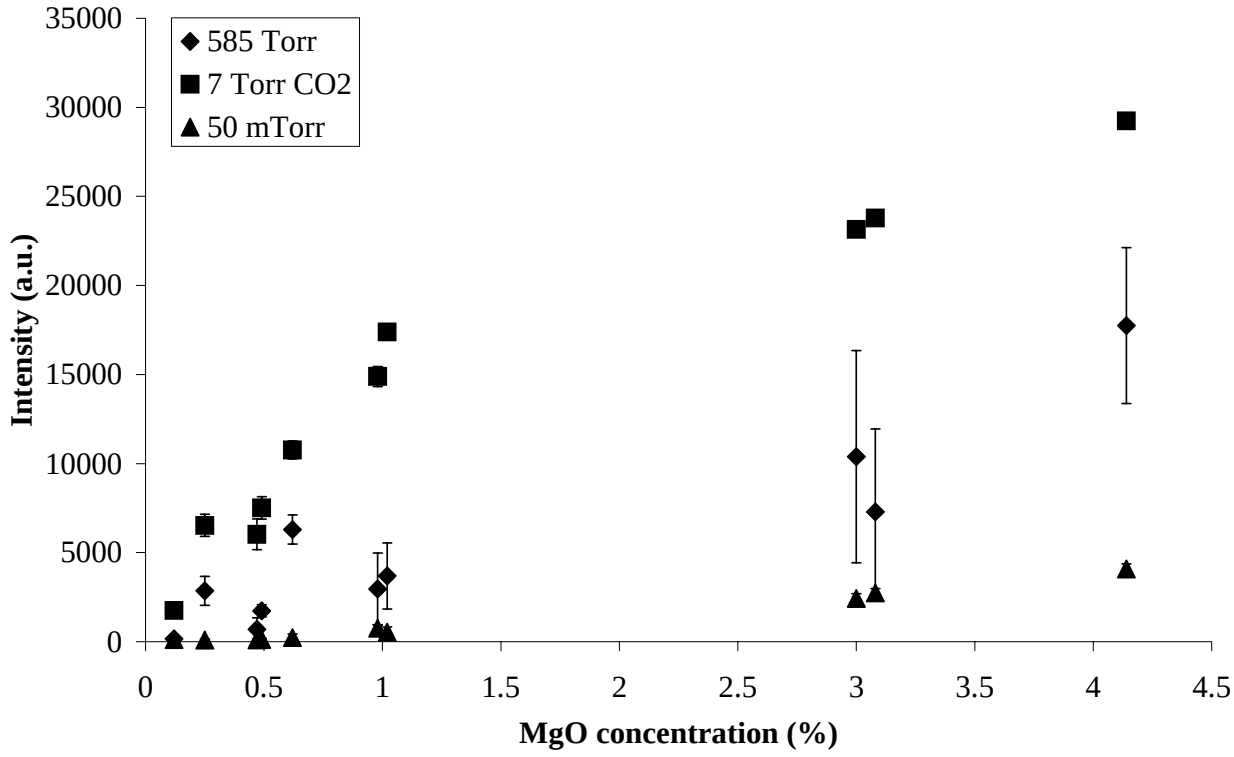

Fig. 8. Calibration curves prepared from soils at different pressures for Mg (280.2 nm) when the optical fibre is placed near the plasma.

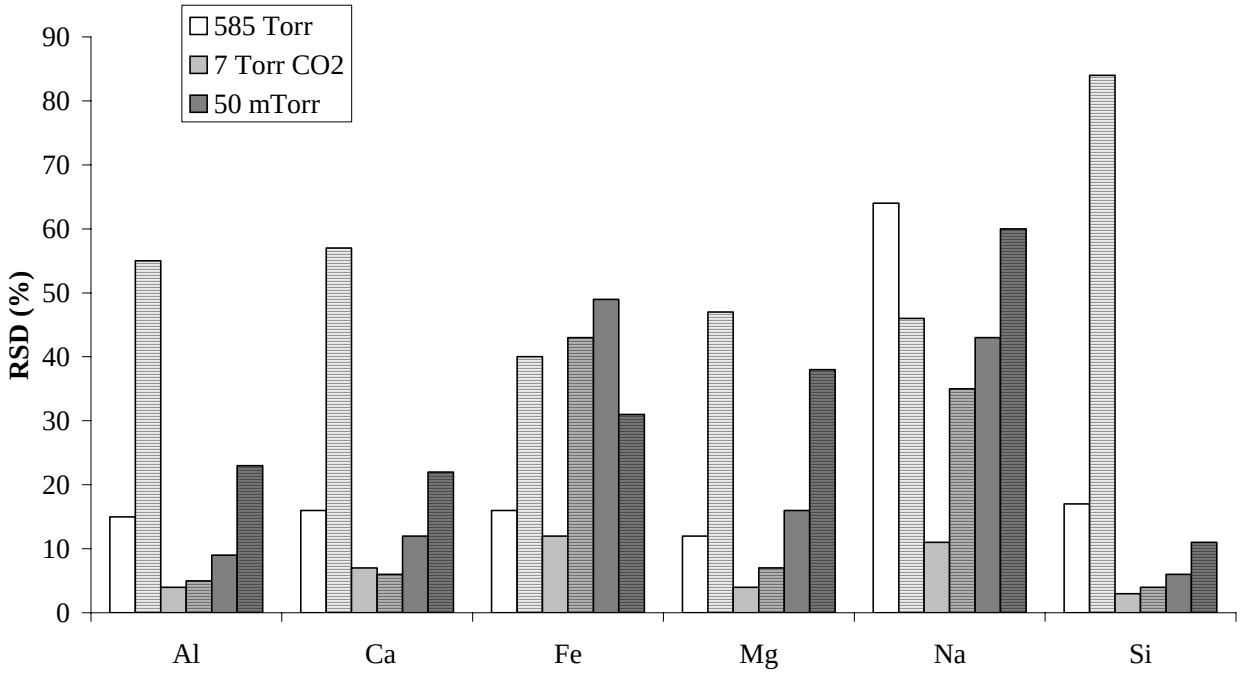

Fig. 9. Relative Standard Deviation (RSD) obtained from calibration curves in soils at three different pressures (no crosshatching corresponds to imaging of plasma light on the optical fibre end and crosshatching corresponds to direct plasma light collection with an optical fibre placed near the plasma).

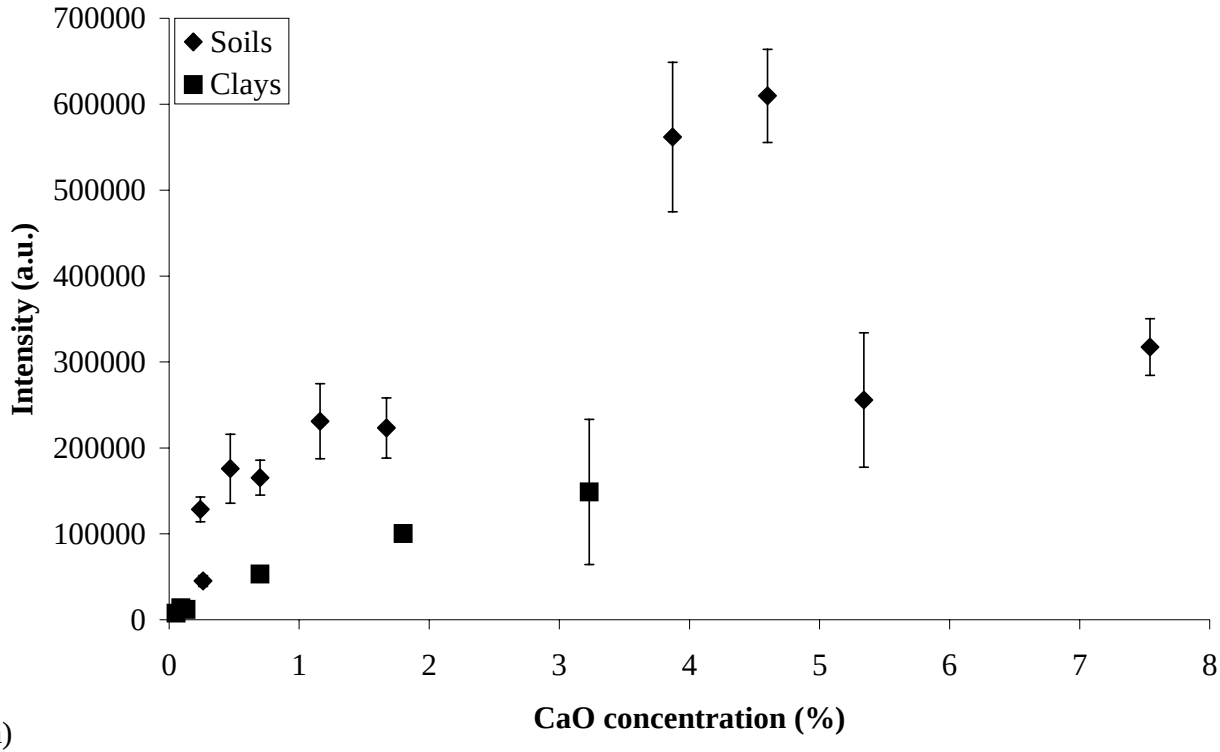
Soils
Clays
Intensity (a.u.)
700000
600000
500000
400000
300000
200000
100000
0
0
1
2
3
4
5
6
7
8
CaO concentration (%)

a)

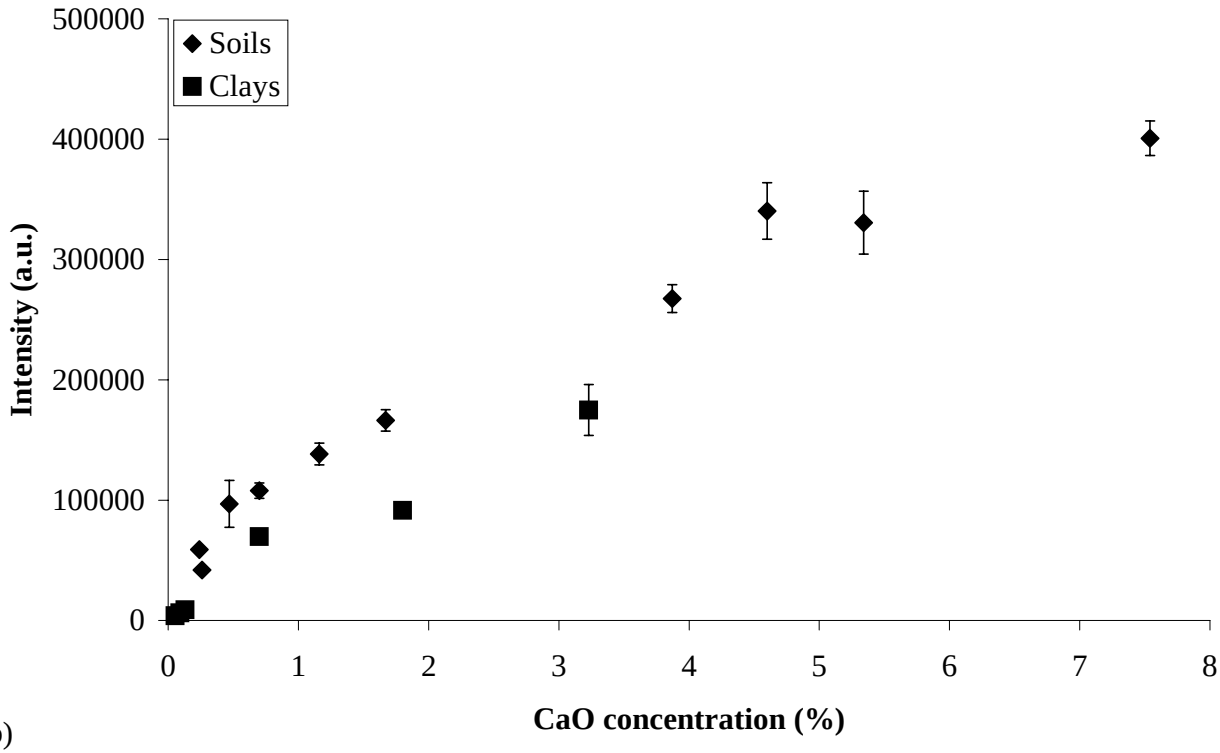
Soils
Clays
Intensity (a.u.)
500000
400000
300000
200000
100000
0
0
1
2
3
4
5
6
7
8
CaO concentration (%)

b)

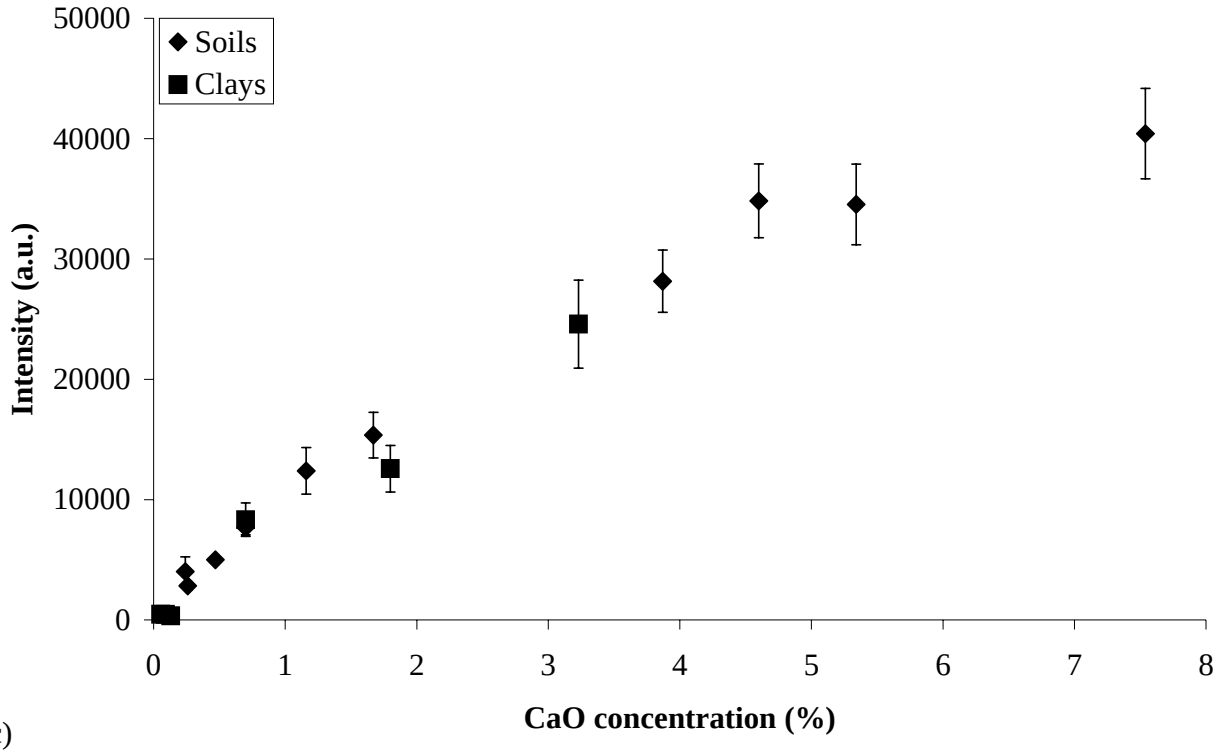

c)

Fig. 10. Calibration curves prepared from certified soils and clays a) at atmospheric pressure; b) at 7 Torr of CO_2 and c) at 50 mTorr.